AGU PUBLICATIONS

JGR

Journal of Geophysical Research: Space Physics

RESEARCH ARTICLE
10.1002/2015JA022293

Key Points:
- ICWs are rarely observed at Titan because of long growth time
- There are two flybys with ICW observed, i.e., T63 and T98
- Simulations are performed to understand the wave growth during T63

Correspondence to:
H. Y. Wei,
hwei@igpp.ucla.edu

Citation:
Russell, C. T., H. Y. Wei, M. M. Cowee, F. M. Neubauer, and M. K. Dougherty (2016), Ion cyclotron waves at Titan, *J. Geophys. Res. Space Physics*, *121*, 2095–2103, doi:10.1002/2015JA022293.

Received 21 DEC 2015
Accepted 15 FEB 2016
Accepted article online 18 FEB 2016
Published online 15 MAR 2016

Ion cyclotron waves at Titan

C. T. Russell[1,2], H. Y. Wei[1,2], M. M. Cowee[3], F. M. Neubauer[4], and M. K. Dougherty[5]

[1]Earth, Planetary, and Space Sciences, University of California, Los Angeles, California, USA, [2]Institute of Geophysics and Planetary Physics, University of California, Los Angeles, California, USA, [3]Los Alamos National Laboratory, Los Alamos, New Mexico, USA, [4]Institute of Geophysics and Meteorology, University of Cologne, Germany, [5]Space and Atmospheric Physics Group, The Blackett Laboratory, Imperial College, London, UK

Abstract During the interaction of Titan's thick atmosphere with the ambient plasma, it was expected that ion cyclotron waves would be generated by the free energy of the highly anisotropic velocity distribution of the freshly ionized atmospheric particles created in the interaction. However, ion cyclotron waves are rarely observed near Titan, due to the long growth times of waves associated with the major ion species from Titan's ionosphere, such as CH_4^+ and N_2^+. In the over 100 Titan flybys obtained by Cassini to date, there are only two wave events, for just a few minutes during T63 flyby and for tens of minutes during T98 flyby. These waves occur near the gyrofrequencies of proton and singly ionized molecular hydrogen. They are left-handed, elliptically polarized, and propagate nearly parallel to the field lines. Hybrid simulations are performed to understand the wave growth under various conditions in the Titan environment. The simulations using the plasma and field conditions during T63 show that pickup protons with densities ranging from 0.01 cm^{-3} to 0.02 cm^{-3} and singly ionized molecular hydrogens with densities ranging from 0.015 cm^{-3} to 0.25 cm^{-3} can drive ion cyclotron waves with amplitudes of ~0.02 nT and of ~0.04 nT within appropriate growth times at Titan, respectively. Since the T98 waves were seen farther upstream than the T63 waves, it is possible that the instability was stronger and grew faster on T98 than T63.

1. Introduction

A pitch angle distribution of ions in which there is a greater flux of energetic ions perpendicular to the field than parallel is generally unstable to the generation of ion cyclotron waves because the resonance of the gyrating ions with such a wave will lead to wave growth and the diffusion of particles to lower pitch angles [*Brice*, 1964], driving the distribution toward isotropy. In a magnetosphere such pitch angle anisotropy is maintained along the field line by a loss cone due to collisions with the atmosphere near the mirror points. This wave generation process may be maintained as long as the particle fluxes remain above a threshold value [*Kennel and Petschek*, 1966]. In a flowing magnetized plasma such as the solar wind, a very strong pitch angle anisotropy may be created and maintained by charge exchange with a neutral gas, such as a planetary exosphere, or through photoionization or impact ionization to the exospheric neutrals in the flowing magnetized plasma. This process was discovered on the Phobos mission as the spacecraft traversed the Mars exosphere [*Russell et al.*, 1990], and waves appeared near the proton cyclotron frequency in the spacecraft frame. Later, such waves were observed in the Earth's exosphere where it was penetrated by the polar cusp [*Le et al.*, 2001].

Strong ion cyclotron waves have also been seen near Io in the Jovian magnetosphere [*Russell et al.*, 1998]. Here the waves were observed over a wide region surrounding Io, much larger than the size of any expected exosphere, signaling the formation of a disk of fast neutrals, produced near Io that populated the surrounding flow plasma torus with ring beam pitch angle distributions of SO_2 and SO ions newly ionized over a radial distance of about 0.5 R_J from Io [*Russell et al.*, 2001; *Wang et al.*, 2001; *Blanco-Cano et al.*, 2001]. Ion cyclotron waves are also seen in the wake region of Europa [*Volwerk et al.*, 2001]

In the Saturnian magnetosphere, these waves were also found, here associated with mass loading of the magnetosphere by the moon Enceladus [*Russell et al.*, 2006], but spread over a greater area than at Io in the Jovian magnetosphere. Here the gas and dust emitted by Enceladus's plume formed what has been called the E ring, which provides a source of ions that are picked up at 90° to the Saturnian field. These ions produced strong waves near the equatorial plane, but the amplitudes fades a few degrees above and below the equatorial plane [*Leisner et al.*, 2011] where the plasma density drops and the wave speed markedly increases. The reduction in magnetic amplitude is consistent with the conservation of the Poynting vector when the wave speed increases.

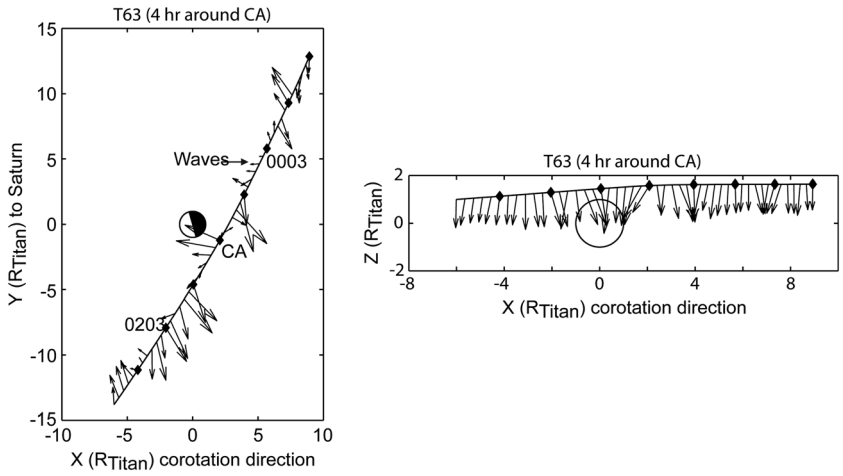

Figure 1. Trajectory of Cassini and projection of magnetic field in equatorial plane on pass T63.

Ion cyclotron waves are not seen in all interactions between a flowing plasma and a neutral atmosphere. Such waves have not been seen above the bow shock at Venus where hot hydrogen and hot oxygen could reach the solar wind flow, but apparently, the flux of such neutrals is insufficient to generate these waves [*Wei et al*., 2011]. In the Saturn magnetosphere, while ion cyclotron waves have been observed at Enceladus, they have not been observed in the interactions with the atmosphereless moons and most surprisingly they were not observed in the initial flybys TA, TB, and T3 of Cassini past Titan [*Neubauer et al*., 2006].

In this paper, we survey the ensuing Cassini flybys of Titan and report the occurrence of waves on Titan passes T63 and T98. We use a hybrid simulation with inputs based on observe plasma parameters to determine why the waves on T63 were observed. Unfortunately, a similar study of the plasma could not be undertaken on pass T98 because the plasma instrument had ceased operations.

2. Observations

The first observations of ion cyclotron waves during a Titan flyby occurred on pass T63, beginning at about 0013 UT on 12 December 2009. The Cassini trajectory is shown in Figure 1, in the plane defined by the radial vector from Titan to Saturn (*Y* axis) and the corotational direction in the nominal direction of the flow in Saturn's direction of rotation (*X* axis). The *Z* axis is parallel to the pole of Titan's orbit (and its rotational axis). Closest approach to Titan is at 0103 UT. Also shown is the magnetic field every 5 min along the orbit as measured by the Cassini fluxgate magnetometer [*Dougherty et al*., 2004]. The spacecraft approaches Titan from inside its orbit and from the downstream side after the flow has made its closest approach to Titan in the northern hemisphere.

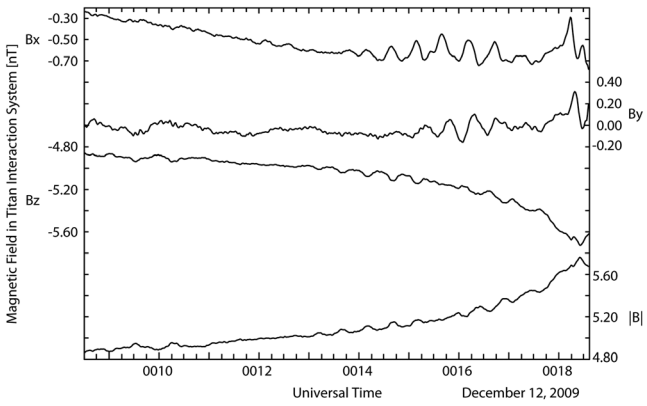

Figure 2. Time series of magnetic field during pass T63. The *x* axis is in the direction of corotation, and the *y* axis is toward Saturn. One second measurements have been used.

The time series of the magnetic field measurements is shown in Figure 2. The coordinate system is in the direction of corotation (*X*), radially toward Saturn (*Y*), and northward (*Z*). The bottom trace shows the field strength and hence is sensitive to only compressional waves. The magnetic field is mainly along the *Z* direction, and hence, the compressional waves are also seen

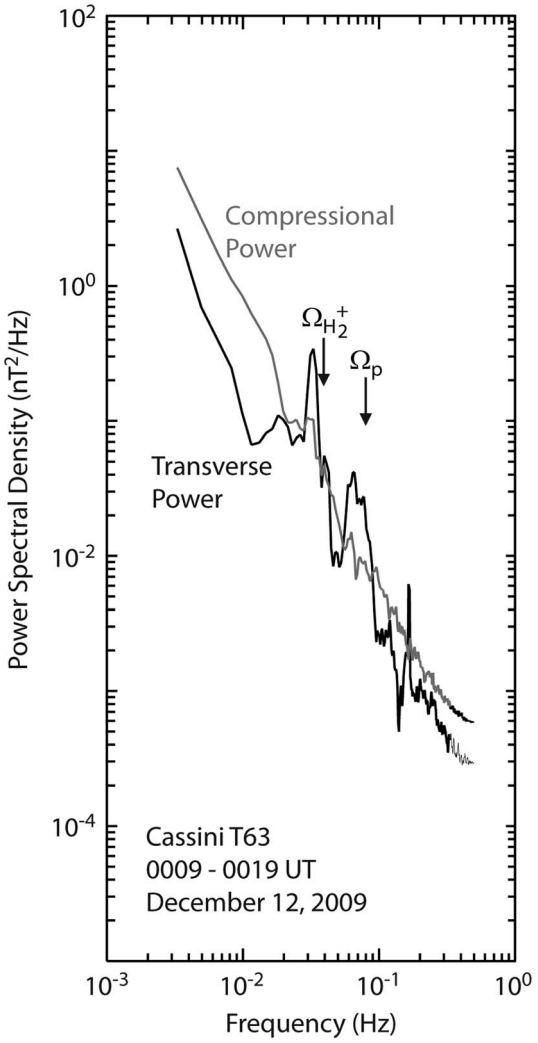

Figure 3. Spectra of compressional and transverse power during pass T63.

clearly on the B_Z component. The compressional waves begin at about 0013 UT and continue to about 0018 UT. The transverse waves begin about 0014 and continue to 0017 UT.

The power spectrum of the compressional component and the transverse component of the wave are shown in Figure 3. The transverse power is computed by subtracting the compressional power from the sum of the powers in the three components measured. The compressional power in the waves is small, consistent with the time series shown in Figure 2 and is mainly in the lower of the two peaks in the spectrum. This peak is just below the molecular hydrogen gyrofrequency. This is precisely the frequency expected to be generated from a pickup ion distribution. This is very clear evidence that molecular hydrogen ions are being picked up by the flow here. The second peak is similar but occurs near the proton gyrofrequency. The power at a slightly higher frequency is most likely due to the burst of signal at the end of the period of waves when the background field is strongest.

A dynamic spectrum of the signals can help determine the temporal behavior of the signal. We use 1 s averages of the data, so our Nyquist frequency is 0.5 Hz as it is in Figure 3. We show in Figure 4 the dynamic spectrum of the magnetic field strength, the compressional power, from 0000 UT to 0019 UT, starting slightly before the interval shown in Figure 2 and analyzed in Figure 3. Each spectrum calculated uses 256 data samples, and a new spectrum is calculated with a 32-point step in time (32 s). Hence, about 35 spectra were used to make Figure 4. The coherence between the *X* and *Y* components (the transverse components) was calculated at each step, and when the coherence was less than 0.4, a black mask was applied to the plot to cover any low statistical accuracy calculations. A coherence of 0.4 is chosen based on prior experience in studying waves in space plasmas. This choice allows us to separate the low coherence noise from the highly coherent signals. The color bar goes from 10^{-3} nT^2/Hz to 10^{-1} nT^2/Hz. The two white lines drawn across the plot mark the instantaneous proton (upper line) and H_2^+ (lower line) gyrofrequencies. There is some compressional noise, but it is mainly in the H_2^+ waves near the end of the interval (i.e., about 0013 to 0018 UT). Figure 5 shows the same display for the transverse component of the power. The transverse and compressional power near the H_2^+ gyrofrequency in the two plots (Figures 4 and 5) peaks around the same frequency and coexists over the same interval with the transverse power being much stronger than compressional. This is consistent with the existence of one wave propagating at an angle to the magnetic field so that it has a small compressional component. For an ideally parallel-propagating ion cyclotron waves (ICW), the wave power is only in the transverse component, while a slightly oblique-propagating ICW could have a compressional power with smaller strength than the transverse power. The H_2^+ wave observed in Figures 4 and 5 appears to be an example of the latter situation.

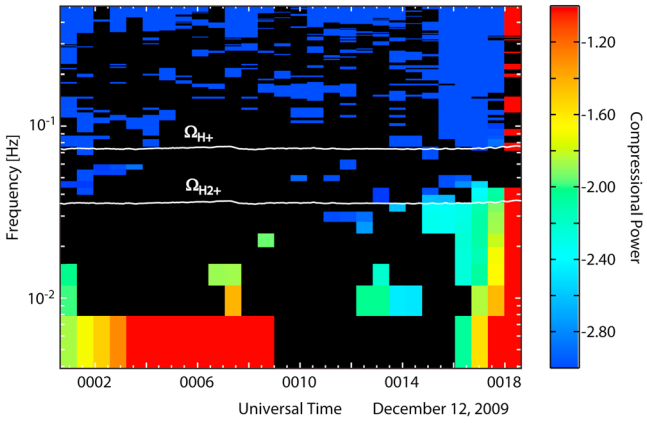

Figure 4. Dynamic spectrum of compressional power during T63. White line shows the gyrofrequencies of proton and molecular hydrogen ions. Each spectrum was created from 256 consecutive 1 s measurements and then shifted by 32 measurements. The power spectral densities were smoothed in frequency by running average of 7 powers at each measurement step. The coherence between the two transverse field components at each estimate of power was calculated, and if the coherence was 0.4 or less, the results were masked in black.

The second observation of ion cyclotron waves was on the T98 flyby. Closest approach to Titan was at 1913 UT. Figure 6 shows two projections of the orbit, in the same coordinate system as in Figures 1 and 2. Cassini approaches Titan from above and downstream. Waves are seen above Titan when the spacecraft is downstream of the body. The magnetic field is drawn every 30 s. The time series of the waves is shown in Figure 7, using 1 s data. Again, the field is oriented mainly along the *Z* direction, so the compressional waves are mainly seen in the *Z* component. Figure 8 shows five power spectra of the compressional and transverse components, each taken over a 5 min interval and covering the interval from 1832 UT to 1857 UT. At first, the compressional power is weak, but it increases with time to become dominant. The compressional fast pressure is below the H_2^+ gyrofrequency, indicating that the power source is pickup of singly ionized molecular hydrogen.

Figure 9 shows the dynamic spectrum of the compressional component of the wave whose upper limit to the power remains a factor of 2 below the proton gyrofrequency. Figure 10 shows the dynamic spectrum of the transverse power. From about 1840 to 1846, it rises in frequency to match the proton gyrofrequency at its highest frequency. This suggests that there is an unstable proton distribution present also.

3. Simulations

To investigate reasons for the appearance of the H^+ and H_2^+ ICW, we carry out 1-D hybrid simulations similar to previous work by *Cowee et al.* [2010]. These simulations can self-consistently reproduce the growth of the ion cyclotron temperature anisotropy instability from a population of pickup ions in the Titan environment, allowing us to better understand the evolution of the instability and the relationship between the wave amplitudes and the pickup ion density. *Cowee et al.* [2010] focused on ICW generated by heavy ions ($m/q = 16$) and identified potential reasons that these ICW have not been observed at Titan, mainly the following: (1) long growth times of these heavy ion waves compared to the convection time of the plasma past Titan and (2) high ambient magnetic field noise especially when Titan is in the plasma sheet. *Cowee et al.* [2010] did hypothesize, however, that ICW generated by the lighter ions, H^+ and H_2^+, which have much shorter growth times, could be seen if their local pickup densities were high enough.

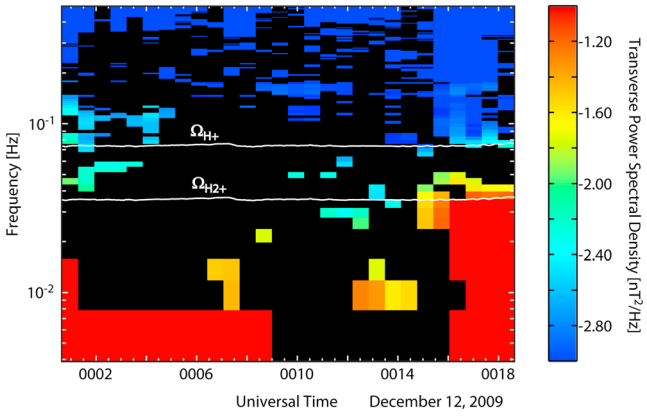

Figure 5. Dynamic spectrum of transverse power during T63. See comments of Figure 4.

For our simulations here, we initialize the system with parameters consistent with observations on T63: ambient magnetic field, B_0, of 5 nT and a perpendicular pickup geometry. We set the nominal pickup velocity of 100 km/s, although the velocities may be slowing as the spacecraft enters the strong

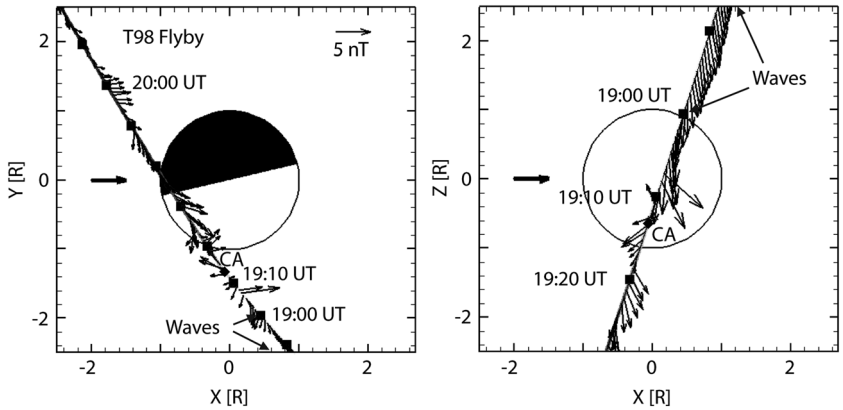

Figure 6. Trajectory of Cassini and projection of magnetic field in (left) equatorial plane and (right) vertical plane along corotation direction on pass T98. Arrows show strength and direction of magnetic field along the trajectory in the plane displayed. Horizontal arrow on left-hand side of each panel shows corotation direction. Closest approach to Titan was at 1913 UT.

mass-loading region (associated with the higher plasma densities in Figure 11). The power spectral density analysis (Figure 3) indicates wave amplitudes of ~0.02 nT ($\delta B/B_0 \sim 0.004$) for H+ and ~0.04 nT ($\delta B/B_0 \sim 0.008$) for H_2^+. Our goal is to estimate the pickup ion densities which yield waves matching these amplitudes.

From integration of the Cassini Plasma Spectrometer (CAPS) time-of-flight measurements [*Thomsen et al.*, 2014] shown in Figure 11, the H^+ and H_2^+ densities are ~0.005 cm^{-3} for several measurement intervals just prior to and at the onset of the ICW observation and then rise by an order of magnitude to ~0.05 cm^{-3} for the measurement just after the ICW observations. Uncertainties in the time-of-flight (TOF) integration, due to the assumption of isotropy in the distribution, are estimated to be no more than a factor of 2 for this interval (M. Thomsen, personal communication, 2015), so we consider the H^+ and H_2^+ ion densities which represent the times of wave growth to be between 0.001 cm^{-3} and 0.1 cm^{-3}. We consider these higher-density values, even though they do not exactly coincide with the time of ICW observation, because it is possible the waves have propagated from a nearby, higher-density location. We do not consider the heavier ions (e.g., water group, N^+ and CH_5^+) in the simulation results shown, because we found they do not play a role in the growth of the lighter H^+ and H_2^+ ICW (not shown).

Despite these constraints on the component densities, we are still left with several unknowns. The pickup ion to background ion relative density is not well quantified in the data but is important because the presence of a background plasma component of the same species as the pickup component will damp the waves. We also do not know if the observed waves are saturated or if they are still growing. *Cowee et al.* [2010] assumed a realistic growth time of ~200 s, which is the transit time of the bulk plasma over an assumed upstream-to-downstream mass-loading region distance of 8 Titan radii (1 R_{Ti} = 2575 km). We may assume this mass-loading region is still roughly appropriate, as the ICW were observed at about 5 R_{Ti} downstream of Titan on T63. This time interval then allows for growth times of ~15 H^+ gyroperiods or ~8 H_2^+ gyroperiods. To more accurately infer growth times, we set the initial noise level in the simulation at $\delta B/B_0 \sim 10^{-3}$, to be consistent with the quieter lobe-like background conditions on T63.

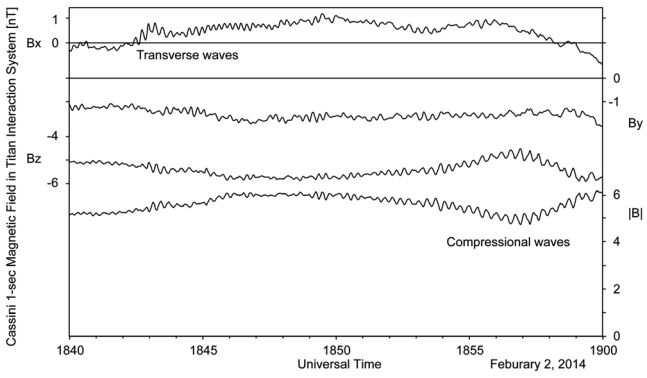

Figure 7. Time series of magnetic field during pass T98. Coordinate system is the same as used in Figures 1, 2, and 6. Corotation is in the positive *x* direction, and the *y* direction is positive inward toward Saturn.

We carry out hybrid simulations to try to identify the pickup ion densities which could have generated the observed ICW amplitudes. The H^+ and H_2^+ instabilities are considered separately, so that the relative contributions to the

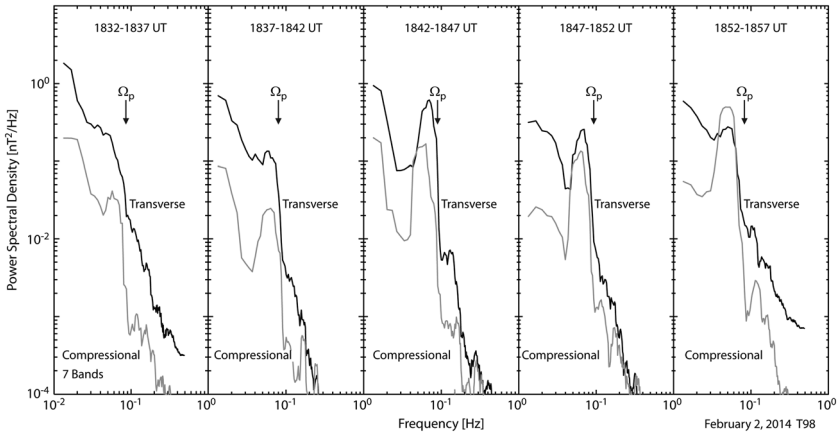

Figure 8. Power spectrum of compressional and transverse powers for five intervals during pass T98. Spectral estimates were smoothed with a running average of length 7. Compressional power obtained from spectral analysis of field strength. Transverse power is the sum of power in each direction, summed with the removal of the power in the field strength. The arrows in each panel mark the proton gyrofrequency.

wave amplitude from each species can be more easily determined. We consider the conditions where all the ions are pickup ions (e.g., no background component), which is the most unstable condition, and we also consider the condition where there is a background component of H^+ or $H_2{}^+$ to damp the waves.

The simulation code treats ions kinetically and electrons as a massless, charge neutralizing fluid [*Winske and Omidi*, 1993]. The simulation has one spatial dimension, x, which is aligned with the background magnetic field, B_0, and fields and velocities are determined in all three dimensions. This is an appropriate setup to reproduce the ion cyclotron temperature anisotropy instability, which has maximum growth at parallel propagation [e.g., *Gary*, 1993]. A standard particle-in-cell technique is used, in which electromagnetic fields are calculated from the densities and currents collected an imposed spatial grid. The plasma is considered to be uniform and homogeneous, containing one or more ion components that are either pickup ions (perpendicular ring, i.e., the parallel velocity nearly zero, $v_{par} \sim 0$, and the perpendicular velocity equals the pickup velocity, $v_{perp} = v_{pickup}$) or background ions (Maxwellian, 100 eV). For simplicity, we carry out initial-value runs, where the pickup ions are all present at the start of the run and the system is then allowed to evolve. We do not inject pickup ions into the simulation over time to mimic ionization as was done in *Cowee et al*. [2010].

Additional simulation input parameters are as follows: normalization $c/V_A = 870$, system length of 120 c/ω_{pi}, 256 grid cells, between 8000 and 64000 superparticles/cell, and time step of 0.05 $\Omega_i{}^{-1}$, in which c is the speed of light, V_A is the Alfven speed, ω_{pi} is the plasma frequency, c/ω_{pi} is ion inertial length, and Ω_i is ion gyrofrequency. Normalized time and spatial scales are proton gyroperiod $(\Omega_i/2\pi)^{-1} = 13.1$ s and intertial length $c/\omega_{pi} = 720.3$ km.

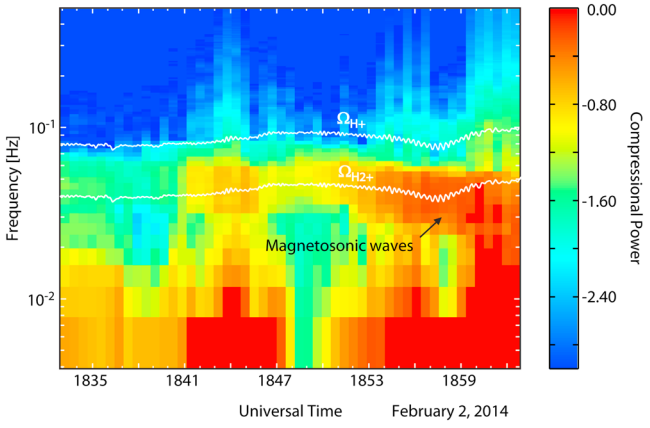

Figure 9. Dynamic spectrum of compressional power during T98 pass. White line shows the gyrofrequencies of proton and molecular hydrogen ions.

Figure 12 shows the time histories of the simulated wave amplitudes for the runs with either the H^+ (top) or $H_2{}^+$ (bottom) instability for varying ring density. Runs where all the ions are pickup ions (e.g., no background component) are indicated by solid lines, and runs for which a background H^+ or $H_2{}^+$ component is added are indicated by the dotted lines. The hypothetical growth time of $\Omega_i t \sim 100$ is marked by the dashed line, and the observed wave amplitude level is marked by the arrow. For the lowest ring densities of ~0.001 cm^{-3} (not

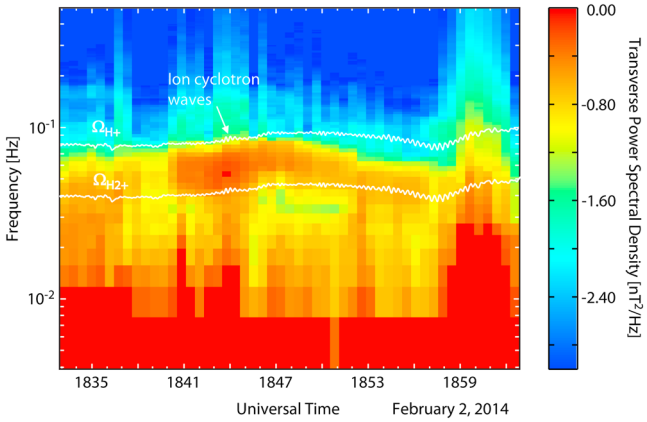

Figure 10. Dynamic spectrum of transverse power on pass T98.

shown), the instability is too weak to produce the observed wave amplitudes but as we increase the ring density to ~0.005 cm^{-3}, the saturation wave amplitudes become larger and may better match the observed wave amplitudes; however, the instability is still weak and the growth times are potentially too long compared to the transit time of the plasma past Titan.

When the ring density is 0.01–0.02 cm^{-3} (all ions are pickup ions, i.e., the solid lines), for H^+ and H_2^+, respectively, we see a good match between the observed wave amplitudes and growth of the waves within a reasonable transit time past Titan. At a given ring density (and pickup velocity), the H_2^+ ring has more initial energy because of its larger mass and drives an instability which saturates at a large wave amplitude. The growth time of the H_2^+ ring is slower than the H^+ ring here because the growth times of the instability scale with the ion gyroperiod. When both of these rings are combined in the simulation, they grow similarly to when they are separate (there are some small interactions between the waves and particles of these similar m/q species but no significant effects), and the simulated power spectral density is shown in Figure 13.

If we had further increased the ring densities to the highest values of 0.1 cm^{-3}, the instabilities would have saturated within $\Omega_i t \sim 100$ but would have had much larger saturation wave amplitudes than is observed. If these densities were realistic, this implies that the waves on T63 were observed during the early times of their growth phase and consequently even higher amplitude waves could have been present further downstream.

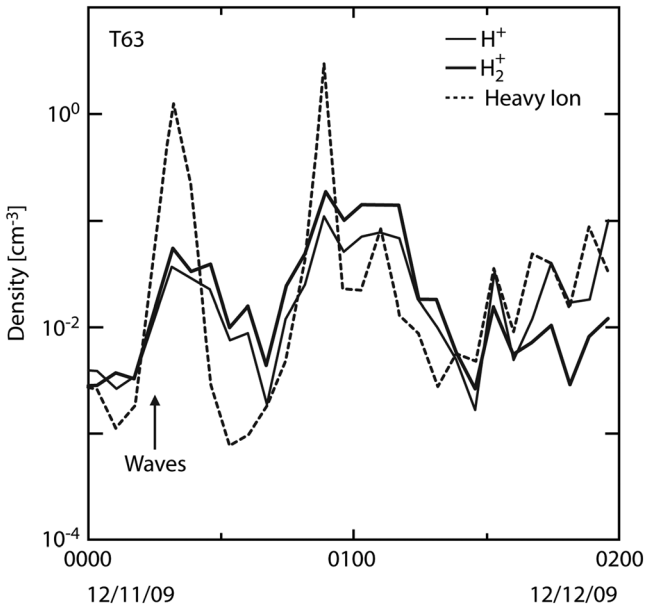

Figure 11. Component densities for T63 inferred from the CAPS TOF integration method of *Thomsen et al.* [2014]. Shown are the H^+, H_2^+, and heavy ion (i.e., $m/q = 16$) densities. The times on the plot represent the start time of the CAPS B cycle observation, taken every 4 min. During this interval, CAPS was looking into the direction of flow, so uncertainty on the densities determined using this TOF integration method should be within a factor of 2. The time when ICWs were observed is indicated on the plot. Plot courtesy Michelle Thomsen.

When we add in a background component of H^+ and H_2^+ in simulations (Figure 12, dotted lines), we find a decrease in the instability growth rate and the saturation amplitude for a given ring density. For these runs, we consider the highest density of 0.1 cm^{-3} to be the total density and apportion it between the ring and background components. In this case, a good match between the simulated and observed wave amplitudes at $\Omega_i t \sim 100$ are found if the ring densities are slightly higher (i.e., ~0.003 ions cm^{-3} more) than for the runs without a H^+ or H_2^+ background present.

4. Conclusions

For the T63 flyby, the 1-D hybrid simulation results indicate that H^+ pickup ion densities ranging from 0.01 cm^{-3} to 0.02 cm^{-3} can drive H^+ ion cyclotron waves with amplitudes of ~0.02 nT within appropriate growth times at Titan. Similarly, H_2^+ pickup ion densities of 0.015 cm^{-3} to 0.25 cm^{-3} can drive H_2^+ ion cyclotron waves with

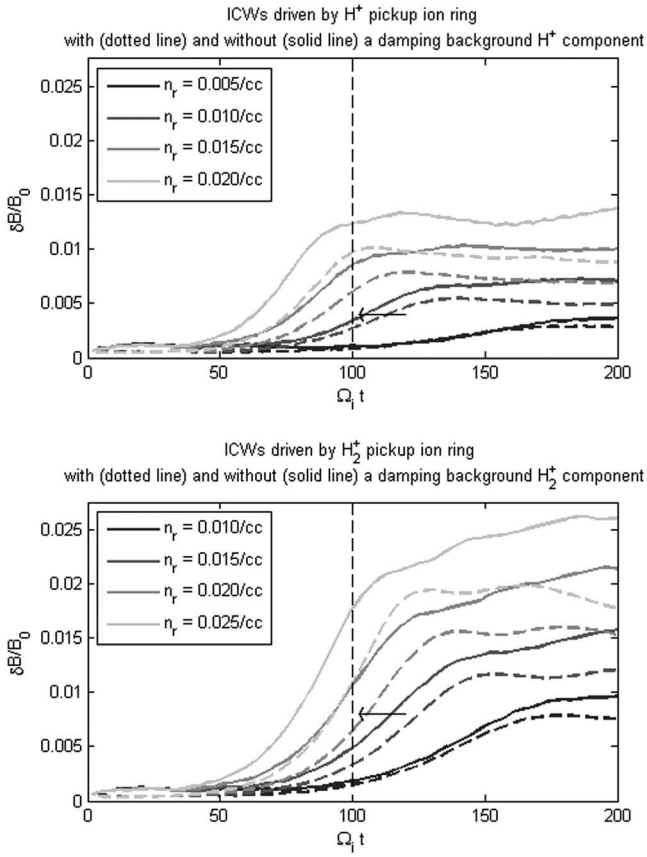

Figure 12. Time histories of the simulated ICW amplitudes for varying pickup ion ring densities (n_r). Instability driven by (top) H^+ and (bottom) H_2^+. Runs with (dotted lines) and without (solid lines) an added background component of H^+ or H_2^+ are shown. The hypothetical growth time of $\Omega_i t = 00$ is indicated by the dashed line, and the observed ICW levels are indicated by the arrows.

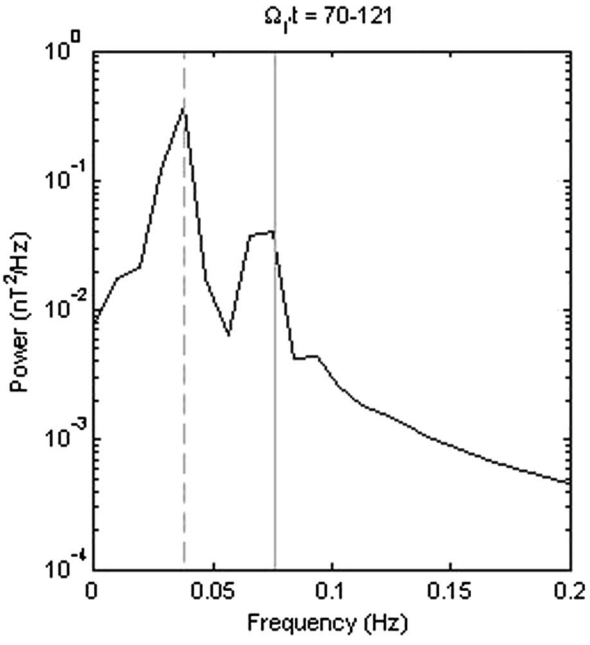

Figure 13. Power spectral density of the simulated H^+ and H_2^+ ICWs. The dashed and solid lines indicate the H_2^+ and H^+ gyrofrequencies, respectively.

amplitudes of ~0.04 nT within appropriate growth times at Titan. Pickup ion densities larger than this can drive even larger amplitude waves, which may be appropriate if the mass-loading region is smaller and thus the allowed growth times are lower. Indeed, because the waves are likely in a state of growth, the assumed size of the mass-loading region is a significant source of uncertainty in these inferred densities.

We note that there are uncertainties in these inferred densities because of assumptions of the nominal pickup velocity and perpendicular pickup geometry in the simulation, as well as possible enhancement of the wave energies due to the one-dimensional nature of the simulation. Additionally, there are uncertainties in the wave amplitudes because they are calculated over only a short

burst interval. Nevertheless, these simulation results combined with the magnetometer observations of the wave spectral properties and the CAPS observations of the light ion component densities demonstrate a consistent picture. Results suggest that the H^+ and H_2^+ pickup ions could have been a dominant component of the plasma at the time of wave observation. Whether or not this would distinguish the T63 pass from other Titan passes is not known, and unfortunately, T98 plasma data are not available.

We can speculate, however, that based on the observed larger wave amplitudes on T98 than T63 and the fact that the T98 waves were seen further upstream than the T63 waves, it is possible that the instability was stronger and grew faster on T98 than T63. The lack of wave observations on the many Titan passes and the short interval of time in which the waves were observed on T63 and T98 suggest that the conditions favorable for strong wave generation are both rare and localized.

Acknowledgments

Work at UCLA was supported by NASA's Cassini project through a subcontract with the Jet Propulsion Laboratory. Work at Los Alamos was supported by NASA grant NNH15AZ13I. Work at Cologne University was supported by internal funds. The Cassini data used in the manuscript are publicly accessible on the Planetary Data System (http://ppi.pds.nasa.gov/search/view/?f=yes&id=pds://PPI/CO-E_SW_J_S-MAG-4-SUMM-1SECAVG-V1.0).

References

Blanco-Cano, X., C. T. Russell, D. E. Huddleston, and R. J. Strangway (2001), Ion cyclotron waves near Io, *Planet. Space Sci.*, *49*(10–11), 1125–1136.

Brice, N. (1964), Fundamentals of very low frequency emission generation mechanisms, *J. Geophys. Res.*, *69*, 4515–4522, doi:10.1029/JZ069i021p04515.

Cowee, M. M., S. P. Gary, H. Y. Wei, R. L. Tokar, and C. T. Russell (2010), An explanation for the lack of ion cyclotron wave generation by pickup ions at Titan: 1D hybrid simulation results, *J. Geophys. Res.*, *115*, A10224, doi:10.1029/2010JA015769.

Dougherty, M. K., et al. (2004), The Cassini magnetic field investigation, *Space Sci. Rev.*, *114*, 331–383.

Gary, S. P. (1993), *Theory of Space Plasma Microinstabilities*, Cambridge University Press, Cambridge.

Kennel, C. F., and H. E. Petschek (1966), Limit on stably trapped particle fluxes, *J. Geophys. Res.*, *71*, 1–28, doi:10.1029/JZ071i001p00001.

Le, G., X. Blanco-Cano, C. T. Russell, X. W. Zhou, F. Mozer, K. J. Trattner, S. A. Fuselier, and B. J. Anderson (2001), Electromagnetic ion cyclotron waves in the high-altitude cusp: Polar observations, *J. Geophys. Res.*, *106*(A9), 19,067–19,079, doi:10.1029/2000JA900163.

Leisner, J. S., C. T. Russell, H. Y. Wei, and M. K. Dougherty (2011), Probing Saturn's ion-cyclotron waves on high-inclination orbits: Lessons for wave generation, *J. Geophys. Res.*, *116*, A09235, doi:10.1029/2011JA016555.

Neubauer, F. M., et al. (2006), Titan's near magnetotail from magnetic field and electron plasma observations and modeling: Cassini flybys TA, TB, T3, *J. Geophys. Res.*, *111*, A10220, doi:10.1029/2006JA011676.

Russell, C. T., J. G. Luhmann, K. Schwingenschuh, W. Riedler, and Y. Yeroshenko (1990), Upstream waves at Mars: Phobos observations, *Geophys. Res. Lett.*, *17*, 897–900, doi:10.1029/GL017i006p00897.

Russell, C. T., M. G. Kivelson, K. K. Khurana, and D. E. Huddleston (1998), Magnetic fluctuations close to Io: Ion cyclotron and mirror mode wave properties, *Planet. Space Sci.*, *47*, 143.

Russell, C. T., X. Blanco-Cano, R. J. Strangeway, Y. L. Wang, and J. Raeder (2001), Evidence for a disk-shaped neutral source cloud at Io, *Adv. Space Res.*

Russell, C. T., J. S. Leisner, C. S. Arridge, M. K. Dougherty, and X. Blanco-Cano (2006), Nature of magnetic fluctuations in Saturn's middle magnetosphere, *J. Geophys. Res.*, *111*, A12205, doi:10.1029/2006/JA011921.

Thomsen, M. F., R. L. Tokar, C. M. Jackman, and R. L. Wilson (2014), Plasma flows in Saturn's nightside magnetosphere, *J. Geophys. Res. Space Physics*, *119*, 4521–4535, doi:10.1002/2014JA019912.

Volwerk, M., M. G. Kivelson, and K. K. Khurana (2001), Wave activity in Europa's wake: Implications for ion pickup, *J. Geophys. Res.*, *106*, 26,033–26,048, doi:10.1029/2000JA000347.

Wang, Y. L., C. T. Russell, and J. Raeder (2001), The Io mass-loading disk: Model calculations, *J. Geophys. Res.*, *106*, 26,243–26,260, doi:10.1029/2001JA900062.

Wei, H. Y., C. T. Russell, T. L. Zhang, and X. Blanco-Cano (2011), Comparative study of ion cyclotron waves at Mars, Venus and Earth, *Planet. Space Sci.*, *59*, 1039–1047, doi:10.1016/j.pss.2010.01.004.

Winske, D., and N. Omidi (1993), Hybrid codes: Methods and applications, in *Computer Space Plasma Physics: Simulation Techniques and Software*, edited by H. Matsumoto and Y. Omura, pp. 103–160, Terra Sci, Tokyo.